Measurement 148 (2019) 106953

Contents lists available at ScienceDirect

Measurement

journal homepage: www.elsevier.com/locate/measurement

An ameliorated synchroextracting transform based on upgraded local instantaneous frequency approximation

Peng Chen [a], Kesheng Wang [a,*], Ming J. Zuo [b,a], Dongdong Wei [a]

[a] Equipment Reliability Prognostics and Health Management Lab (ERPHM), School of Mechanical and Electrical Engineering, University of Electronic Science and Technology of China, Chengdu 611731, PR China
[b] Department of Mechanical Engineering, University of Alberta, Edmonton, Alberta T6G 1H9, Canada

ARTICLE INFO

Article history:
Received 8 March 2019
Received in revised form 19 July 2019
Accepted 15 August 2019
Available online 21 August 2019

Keywords:
Time-frequency analysis (TFA)
Reassignment method (RM)
Instantaneous frequency (IF) estimation
Synchroextracting Transform (SET)

ABSTRACT

This paper introduces an upgraded synchroextracting transform (SET), namely ameliorated synchroextracting transform (ASET), to deal with fast time-varying and strong frequency modulated signals for time and frequency analysis (TFA). SET is a recently developed time-frequency representation (TFR) method with an exceptional capability to enhance the readability of TFR, yet the kernel of SET is based upon the assumption of purely harmonic signal, therefore, it is more applicable to slow time-varying and weekly frequency modulated signals. However, for rotating machines in real practice, fluctuation loads and varying rotational speeds are always inevitable, the resultant vibrations will exhibit non-stationary frequency-modulated nature. To tackle this problem, in this paper, the synchroextracted operator in SET is upgraded in terms of second-order Taylor expansion to estimate the fast and strong frequency modulated signals so that a better TFR can be achieved. The advantages of ASET is demonstrated with simulated and experimental studies by comparing the existing time and frequency analysis methods. The sharpness of TFR, the ability of signal reconstruction and the robustness to noise pollution are also demonstrated.

1. Introduction

Time-frequency analysis (TFA) has been widely used in a wide variety of fields such as speech, mechanical vibration, electromagnetic equipment and radar signals [1–4]. The classical TFA methods, such as short-time Fourier transform (STFT) [5], Wigner-Ville distribution (WVD) [6] and continuous wavelet transform (CWT) [7], all have their inherent drawbacks. For STFT, due to the invariable width of each analyzed window, it suffers from poor time-frequency (TF) resolution which limits the ability of the method to represent features of non-stationary signals. Restricted by the cross-terms when analyzing multicomponent signals, WVD may result in illusive components [8]. In detecting the ridges, or in other words, tracking the instantaneous frequencies from CWT result [9], for non-stationary signal, the blurred TFR may also occur and the readability of the TF spectrum is therefore not satisfactory for ridge detection.

Time-frequency analysis is heavily dependent on clear TFR results, i.e., energy concentrated or sharpened representation and no misleading interference terms in TF plane. TFR, especially the high-quality TF readability, is beneficial for visual interpretation of TFA results as well as better discrimination between known patterns for non-stationary signal classification.

However, as have been mentioned above, it should notice that the traditional TFA methods all have limitations on their TF readability. Therefore, in order to obtain a high-resolution of TF readability, some post-processing TF technique is developed. Recently, advanced TFA approaches such as reassignment method (RM) [10], synchrosqueezing transform (SST) [11,12] and synchroextracting transform (SET) [13], have been proposed. Among them, RM reassigns the time-frequency spectrogram into the instantaneous frequency (IF) trajectory along with the two-dimensional TF directions, an improved energy concentration of TFR, therefore, can be provided. However, it loses its ability to reconstruct the components from the original signal [14]. In order to solve the signal reconstruction problem, the method of SST is proposed. SST squeezes the TF coefficients into the IF trajectory only in the frequency direction, as a result, it can not only exhibit a TF spectrum with better readability, but also can provide the reconstruction ability to extract a specific component from the original signal. By comparing STFT, CWT and the recently introduced SST, Iatsenko D et al. [15,16] found that SST also has its drawbacks in low TF resolution of separating and reconstructing

* Corresponding author.
E-mail address: keshengwang@uestc.edu.cn (K. Wang).

https://doi.org/10.1016/j.measurement.2019.106953
0263-2241/

the interesting components from the raw signal and is highly sensitive to noise. For solving the above shortcomings and providing a high-resolution TFR, SET is proposed by Yu et al. [13]. The strategy of SET is to retain the closest information related to time-varying features of the original signal and reduce the blurred TF energy in TFR. As a result, it can provide a high-resolution TFR with signal reconstruction ability and simultaneously it features red an improved robust to noise pollution. Though the SET features several advantages, it also has limitations on representing signals with nonlinear and non-stationary nature. The main reason for that is the standard SET based upon the assumption that the analyzed signal is purely harmonic [17,18]. As a result, it is more applicable to deal with signals with "small" amplitude and frequency modulations, whereas, signals with "strong" nonlinear and non-stationary nature are of not suitable for the current SET method. In other words, SET is incapable to deal with strong nonlinear and non-stationary signal properly. In fact, most signals, may feature nonlinear and non-stationary nature, such as, chirps involved in radar [19], voice signal [20], oscillatory waves [21], and vibration signal of rotating machinery [22–24]. To overcome this problem, various technical approaches have been addressed on how to deal with fast and strong frequency modulated signal. For instance, in [25], a generalized synchrosqueezing algorithm is introduced, and it is composed of two distinct steps: first of which is computes SST, estimates the instantaneous frequency modulation, and the second part can be described in terms of recomputes SST on the demodulated signal. Similarly, an iterative procedure algorithm is developed in [26,27], where at each iteration, SST is computed with a better time-frequency resolution. In our preliminary work [28], a generalized synchroextracting transform (GSET) designed of the hybrid a synchroextracting operator and a generalized Fourier transform, and it has been successfully applied to enhance the time-frequency representation for a similar type of signal analysis. For GSET, it is sensitive to noise, as a result, it is not suitable to deal with a noise-contaminated signal in real practice. And, for GSET, the procedure of generalized Fourier transform (GFT) is always needed. Multiple iterations procedures in GFT are essential to obtain an instantaneous phase function which is used to decompose the original signal. However, a best-matched instantaneous phase function, especially for the fast and strong modulated signal, is not easy to be obtained by these multiple iteration procedures.

In contrast with all the above mentioned attempts [25–28], in this paper, a one-step ameliorated synchroextracting transform (ASET) is proposed. It consists of an improved version of the local instantaneous frequency estimation (LIFE) for SET and then the synchroextracting operator is applied to rearrange the coefficients of the STFT. Compared with reported SET methods using the synchroextracting operator, ASET utilizes a second-order approximation strategy to upgrade SET to deal with the noted fast and strong modulation signal. In principle, these methods can be divided into two categories. The first type is multiple iterations (multiple steps) algorithm which is mentioned in [25–28]. And the second type is a one-step algorithm such as [10,11,13]. The synchrosqueezing operator in first type methods is based upon the assumption of a purely harmonic signal. However, the proposed ASET method as a one-step algorithm is based on the improved version of a kernel of LIFE to deal with the fast and strong modulated signal. For fair comparison's sake, ASET will be compared with traditional TFA methods such as STFT, RM and recently proposed the one-step algorithm SST and SET. In the end, ASET is validated by synthetic and experimental rotating machine vibration signal.

The remainder of this paper is structured as follows: firstly, in Section 2, we will revisit the basic theory of SET and then the limitations of the standard SET will be illustrated in Section 3. In Section 4, the numerical experiments and performance exploration will be delivered. Besides, two numerical signals are applied to illustrate the quantified analysis of the TF representation by different TFAs. The applications of mechanical vibration signal analysis could be found in Section 5. Finally, the conclusion could be drawn in Section 6.

2. Revisiting the synchroextracting transform for TFR

Using STFT to analyze multi-component signals, when it comes to a distance between two ridges in TFR is not larger than the width of the frequency support of window g and then each of the components is occupied overlapping regions in the TF plane [11,29]. As a result, the readability of the time-frequency spectrum is dropped tremendously and it means that the corresponding TFR energy is smeared and may mislead to the misleading signal analysis result. To alleviate the TFR blurring effect from the result of STFT, Ingrid Daubechies et al. [11] introduced the algorithm of synchrosqueezing. Furthermore, to obtain a more ideal and energy concentrated TFR, Yu et al. [13] proposed a synchroextracting transform. In this method, it used a post-processing operator, namely synchroextracting operator, to obtain the IF information most related to time-varying features of the original signal and, to a large extent, remove smeared TF energy, thus the energy concentration of TFR can be enhanced. In the following, the mathematical theory of SET will be briefly reviewed.

Suppose that the signal is a purely harmonic signal [13] $x(t) = A(t)e^{2i\pi\phi(t)}$ i.e., a constant frequency $\phi'(t) = f_0$ and with invariant amplitude $A(t) = A_0$,

$$x(t) = A_0 e^{i2\pi f_0 t} \tag{1}$$

The Fourier transform (FT) of $x(t)$ can be obtained as,

$$\hat{x}(f) = A_0 \cdot \delta(f - f_0) \tag{2}$$

The following *four* steps are necessary.

Step 1: To obtain the result of STFT. $S_x^g(t,f)$ denotes STFT of the original signal $x(t)$ using the analyzed window g, and it can be calculated as,

$$\begin{aligned} S_x^g(t,f) &= \int_0^{+\infty} x(u)g(u-t)e^{-i2\pi f(u-t)}du = M_x^g(t,f)\cdot e^{2i\pi\phi_x^g(t,f)} \\ &= A_0 \cdot \hat{g}(f-f_0)\cdot e^{i2\pi f_0 t} = x(t)\cdot \hat{g}(f-f_0) \end{aligned} \tag{3}$$

Remark: The usual definition of STFT differs from Eq. (3) by a factor $e^{2i\pi ft}$. Also, as we assume the analyzed window function g to be real-valued. Where $\hat{g}$ is the FT of g. $M_x^g(t,f)$ is instantaneous amplitude of STFT result with $x(t)$ and the instantaneous frequency f_0 of STFT with $x(t)$ holds $f_0 = \frac{\partial\left(\phi_x^g(t,f)\right)}{\partial t}$.

Step *2*: To obtain the estimation of instantaneous frequency, it is based on the result of step *1* and calculate the derivative of $S_x^g(t,\omega)$ with respect to time as,

$$\omega_{ins}(t,f) = \phi'(t) = \partial_t\phi_x^g(t,f) = \frac{1}{2\pi}\partial_t arctan S_x^g(t,f) = \frac{1}{2i\pi}\frac{\partial_t S_x^g(t,f)}{S_x^g(t,f)} \tag{4}$$

where $\omega_{ins}(t,f)$ is the estimation of IF for $x(t)$.

Step *3*: To reassign the complex coefficients on STFT result. Reassignment details of mapping $(t,f)\rightarrow(t,\omega_{ins}(t,f))$ reader may refer to [13],

$$T_e^x(t,f) = S_x^g(t,f)\cdot\delta(\omega-\omega_{ins}(t,f)) \tag{5}$$

where $T_e^x(t,f)$ denotes SET of $x(t)$.

Step 4: To reconstruct the original signal $x(t)$. Substituting Eq. (3) into Eq. (5), as such $x(t)$ can be obtained by,

$$x(t) = \frac{1}{\hat{g}(\omega-\omega_0)\cdot\delta(\omega-\omega_{ins}(t,f))}\Big|_{\omega=\omega_0,\ \omega=\omega_{ins}(t,f)} \cdot \int_0^{+\infty} T_e^x(t,f)df = \frac{1}{\hat{g}(0)}\cdot\int_0^{+\infty} T_e^x(t,f)df \tag{6}$$

To illustrate the TF representation and reconstruction results of different TFA methods, a numerical synthetic signal $x(t)$ is used for demonstration. This signal consists of four components, that is a pure harmonic $x_1(t)$, a linear chirp signal $x_2(t)$, a small variation frequency modulated signal $x_3(t)$ and a strongly nonlinear sinusoidal frequency modulated signal $x_4(t)$. The waveform of $x(t)$ and its Fourier spectrum are presented in Fig. 1(a) and (b), respectively. The ideal TF trajectories are displayed in Fig. 1(c). Using STFT, SST, SET and RM to analyze signal of $x_1(t), x_2(t)$ and $x_3(t)$, the corresponding TFRs are plotted in Fig. 2(a), (b), (c) and (d). It is clearly shown that the results of STFT and SST generates smeared TFR, but $x_1(t)$ can precisely exhibit by SST (see in Fig. 2(b)). Comparing the TFRs from SET and RM, it can be found that the first three modes are perfectly represented in a sharpened TF trajectories (see in Fig. 2(c) and (d)). Owing to the mode $x_4(t)$ consisting strongly non-stationary frequency modulation, it leads to substantially distorted IF trajectories (see in Fig. 2(a), (b), (c) and (d)) as compared to the ideal IF trajectories shown in Fig. 1(c). The above discussions can be briefly illustrated by Table 1.

The above observations motivate us to tackle the strongly frequency-modulated mode in signal analysis. To obtain a clear TFR or precisely represent strong time-varying frequency modulation features of signals, an ameliorated synchroextracting transform (ASET) approach is then introduced to cope with this problem.

3. Ameliorated synchroextracting transform (ASET)

In Section 2, it is known that SET is based on an assumption of pure harmonic signal, i.e., containing "small" frequency modulations. It can be described as, for all t and $\forall\varepsilon>0, |A'(t)|\leqslant\varepsilon$ and $|\phi''(t)|\leqslant\varepsilon$. To accommodate strong frequency modulation, an upgraded local instantaneous frequency approximation is used to modify the approach of ASET, and the mathematical theory of ASET will be given in this Section.

Let us consider a signal $h(t)=B(t)e^{2i\pi\phi(t)}$, where $\phi(t)=a+bt+\frac{1}{2}ct^2$ is a polynomial of degree 2 and $B(t)>0$. It is also possible to choose other higher degree. Yet, they all have similar analysis. Thus, in this paper we use second-order degree as an example. To apply SET to a signal $h(t)$, step *1*, the STFT result of $S_h^g(t,f)$ should be calculated first. For this signal, $\phi'(t)$ is not a constant anymore, thus a second-order Taylor expansion is used to approximate the phase function $\phi(t)$ at t,

$$\begin{aligned} h(u) &= B(u)e^{2i\pi\phi(u)} = B(t)e^{2i\pi\left(a+bt+\frac{1}{2}ct^2\right)}\Big|_{u=t} \\ &= B(t)e^{2i\pi\left[\phi(t)+\phi'(t)(u-t)+\frac{1}{2}\phi''(t)(u-t)^2\right]} \\ &= B(t)e^{2i\pi\phi(t)}\cdot e^{i\pi\phi''(t)(u-t)^2}e^{2i\pi\phi'(t)(u-t)} \\ &= h(t)\cdot e^{i\pi c(u-t)^2}e^{2i\pi\phi'(t)(u-t)} \end{aligned} \tag{7}$$

Step 1: Note that $\phi''(t)=c$ and substitute Eq. (7) to (3) with $u-t=\tau$, then the STFT of signal $h(t)$ can be calculated as,

$$\begin{aligned} S_h^g(t,f) &= \int_0^{+\infty} h(u)g(u-t)e^{-i2\pi f(u-t)}du \\ &= \int_0^{+\infty} h(t)\cdot e^{i\pi c(u-t)^2}e^{2i\pi\phi'(t)(u-t)}g(u-t)e^{-i2\pi f(u-t)}du \\ &= h(t)\int_0^{+\infty} g(\tau)e^{i\pi c\tau^2}e^{-i2\pi\left(f-\phi'(t)\right)\tau}d\tau = M_h^g(t,f)\cdot e^{i\cdot\phi_h^g(t,f)} \end{aligned} \tag{8}$$

where $M_h^g(t,f)$ and $\phi_h^g(t,f)$ are instantaneous amplitude and instantaneous phase of STFT result with $h(t)$, respectively.

In [30], it was shown that the local time delay $\hat{t}_{ins}(t,f)$ can be used to calculate the instantaneous frequency and it was also defined in [31]. As such, in the case of signal $h(t)$, the $\hat{t}_{ins}(t,f)$ can be written as,

$$\hat{t}_{ins}(t,f) = t - \frac{1}{2\pi}\frac{\partial\phi_h^g(t,f)}{\partial f} = t - \frac{1}{2\pi}\partial_f\ arg\ S_h^g(t,f) \tag{9}$$

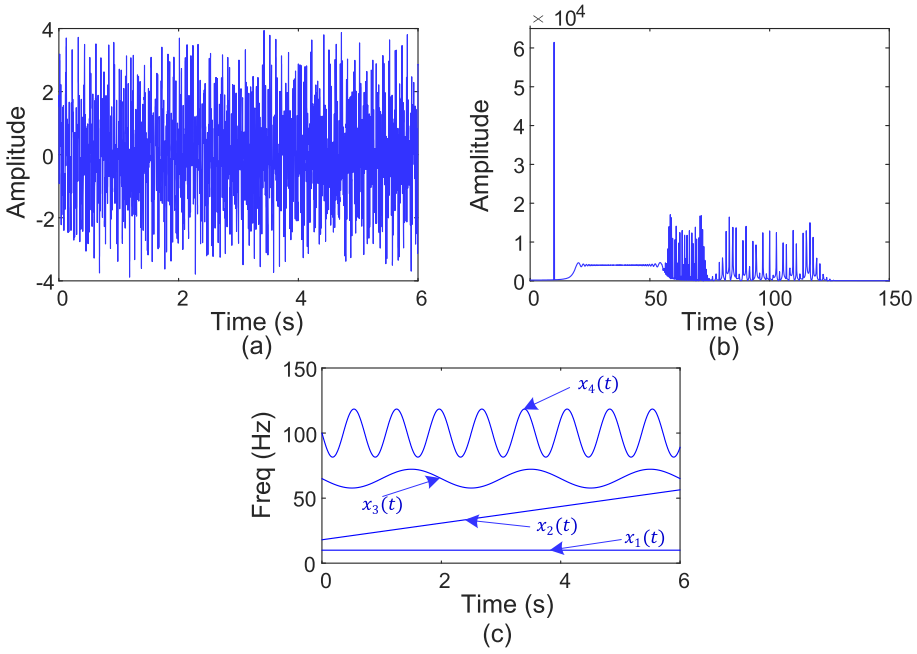

Fig. 1. (a) Waveform of simulated signal (b) Fourier spectrum of simulated signal (c) Ideal IF, $x_1(t)=\sin(2\pi\cdot 10t)$; $x_2(t)=\sin(2\pi\cdot(18t+3.2t^2))$; $x_3(t)=\sin(2\pi\cdot(65t+2.3\cdot\cos(2\pi\cdot 0.5t)))$; $x_4(t)=\sin(2\pi\cdot(100t+2.1\cdot\cos(2\pi\cdot 1.4t)))$.

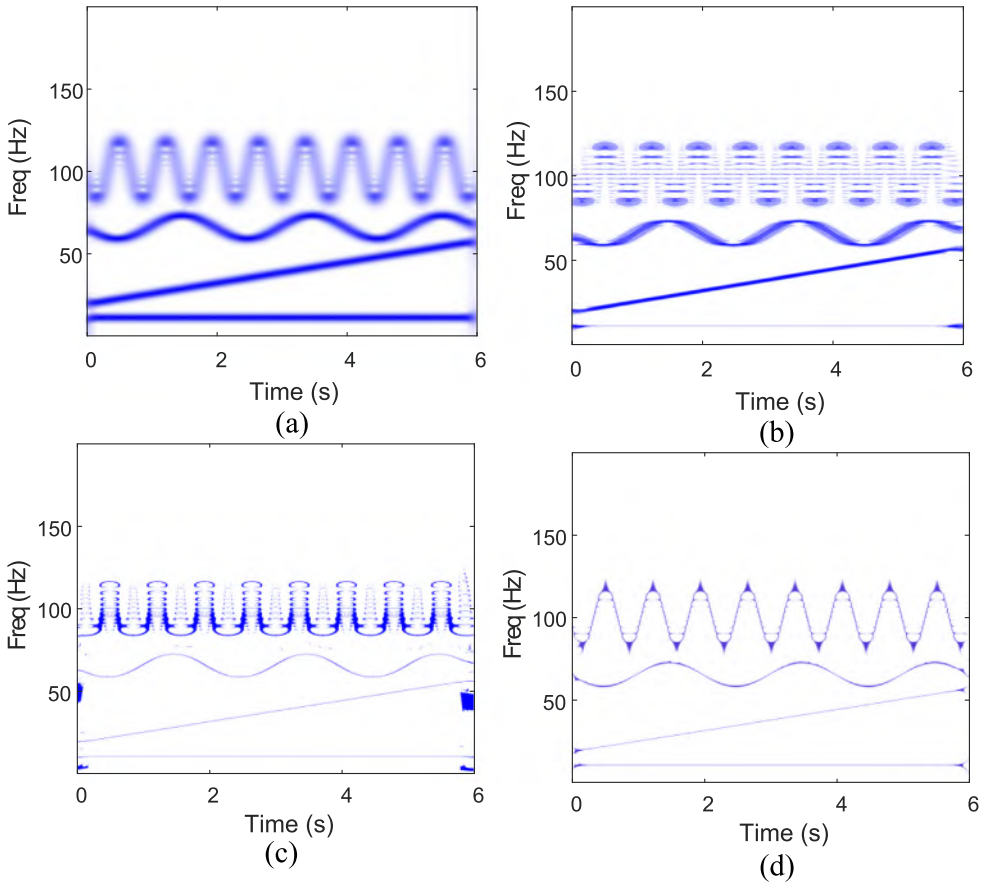

Fig. 2. (a) Time-frequency spectrum: STFT result, (b) SST result, (c) SET result, (d) RM result.

Table 1
Performance of different methods for TFA.

TFA methods	TFR[a] for $x_i(t)$ $(i = 1 \sim 4)$				Reconstruction[b]
	$x_1(t)$	$x_2(t)$	$x_3(t)$	$x_4(t)$	
STFT	B	B	B	B	R
SST	C	B	B	B	R
SET	C	C	C	B	R
RM	C	C	C	B	Non-r

[a] B means that the TFR is blurred, C denotes that the TFR is clear.
[b] R (or Non-r) means that this method have (or do not have) the ability to reconstruct interested signal.

where $\phi_h^g(t,f)$ is the phase function of signal $h(t)$. Substituting Eq. (8) into Eq. (9), $\hat{t}_{ins}(t,f)$ can be obtained as,

$$\begin{aligned}\hat{t}_{ins}(t,f) &= t - \frac{1}{2\pi}\partial_f \, arg\left[h(t)\int_0^{+\infty} g(\tau)e^{i\pi c\tau^2}e^{-i2\pi\left(f-\phi'(t)\right)\tau}d\tau\right] \\ &= t - \frac{1}{2\pi}\partial_f\left[2\pi\phi(t) + arg\int_0^{+\infty} g(\tau)e^{i\pi\phi''(t)\tau^2}\cdot e^{-2i\pi\left(f-\phi'(t)\right)\tau}d\tau\right] \\ &= t - \frac{1}{2\pi}\partial_f \, arg\int_0^{+\infty} g(\tau)e^{i\pi\phi''(t)\tau^2}\cdot e^{-2i\pi\left(f-\phi'(t)\right)\tau}d\tau \end{aligned} \tag{10}$$

Assuming the function of u was defined as,

$$u(\xi) = \frac{d}{d\xi} arg\left\{\int_0^{+\infty} g(x)e^{i\pi\phi''(t)x^2}e^{-2i\pi\xi x}dx\right\} \tag{11}$$

Then $\hat{t}_{ins}(t,f)$ can be given in a simplified form as,

$$\hat{t}_{ins}(t,f) = t - \frac{1}{2\pi}u(f-\phi'(t)) \tag{12}$$

The estimation of the instantaneous frequency ϕ' is given by [31],

$$\hat{\omega}_{ins}(t,f) = \phi'\left(\hat{t}_{ins}(t,f)\right) \tag{13}$$

Recalling that $\phi'(t) = b + ct$, then $\hat{\omega}_{ins}(t,f)$ can be obtained by

$$\begin{aligned}\hat{\omega}_{ins}(t,f) &= b + c\cdot\hat{t}_{ins}(t,f) = b + ct - \frac{c}{2\pi}u(f-\phi'(t)) \\ &= \phi'(t) - \frac{c}{2\pi}u(f-\phi'(t))\end{aligned} \tag{14}$$

Eq. (14) clearly shows that,

Case *1*: if $c = \phi''(t) = 0$, it mean that $\hat{t}_{ins}(t,f)$ is identical with Eq. (4), therefore SET is valid.

Case *2*: if $c = \phi''(t) \neq 0$, SET is not valid, yet Eq. (14) cannot hold this condition. Hence, we introduce second-order Taylor expansion and the instantaneous frequency can be approximated as,

$$\begin{aligned}\phi'(t) &= \phi'\left(\hat{t}_{ins}(t,f)\right) + \phi''\left(\hat{t}_{ins}(t,f)\right)\left(t - \hat{t}_{ins}(t,f)\right) \\ &= \omega_{ins}(t,f) + \hat{q}_h(t,f)\left(t - \hat{t}_{ins}(t,f)\right)\end{aligned} \tag{15}$$

Letting $\phi''\left(\hat{t}_{ins}(t,f)\right) = q_h(t,f)$, and it was defined as followings,

$$\hat{q}_h(t,f) = Re\left\{\frac{\partial_t\left(\frac{\partial_t S_h^g(t,f)}{S_h^g(t,f)}\right)}{2i\pi - \partial_t\left(\frac{\partial_f S_h^g(t,f)}{S_h^g(t,f)}\right)}\right\} \tag{16}$$

Step 2: In [30,32] the local operator $\hat{q}_h(t,f)$ has been given. Therefore, the upgraded estimation of the local instantaneous frequency can be written as follows,

$$\tilde{\omega}_{ins}(t,f) = \omega_{ins}(t,f) + \hat{q}_h(t,f)\left(t - \hat{t}_{ins}(t,f)\right) \tag{17}$$

Step 3: Ameliorated synchroextracting transform (ASET) is then determined by replacing $\omega_{ins}(t,f)$ in Eq. (5) with $\tilde{\omega}_{ins}(t,f)$, and defines as,

$$\widetilde{T}_e^h(t,\omega) = S_x^g(t,f)\cdot\delta(\omega - \tilde{\omega}_{ins}(t,f)) \tag{18}$$

where $\omega = 2\pi f$ and $\widetilde{T}_e^h(t,\omega)$ denotes ASET of $h(t)$.

Step 4: Meanwhile, the component of $h(t)$ can also be reconstructed by replacing $T_e^x(t,\omega)$ with $\widetilde{T}_e^h(t,\omega)$ in (6) as following,

$$x(t) = \frac{1}{\hat{g}(0)}\cdot\frac{1}{2\pi}\int_0^{+\infty}\widetilde{T}_e^h(t,\omega)d\omega \tag{19}$$

Thus, Eq. (8) of step 1, Eq. (17) of upgraded step 2, Eq. (18) and Eq. (19) of step 3 and 4, makes up the ameliorated synchroextracting transform.

From the SET method demonstrated in Section 2 and the proposed ASET derived in Section 3, it can be concluded that SET is based on the pure harmonic signal, i.e., containing "small" frequency modulation, so the instantaneous frequency can be estimated by the Eq. (4) and the TFA results of $x_1(t), x_2(t)$ and $x_3(t)$ are well represented by SET as it shown in Fig. 2(c). However, for the strong frequency modulated signal $x_4(t)$ in Fig. 2(c), it can be noted that the smeared time-frequency energy is not converged into TF trajectory so it causes an ambiguous TFA result. And the TF information cannot be precisely extracted from this result as well. Therefore, the standard SET is not suitable for analyzing this type of strong frequency modulated signal. To accommodate the strong frequency modulated signal, the current instantaneous frequency approximation in Eq. (4) need to be upgraded, so the new instantaneous frequency estimation theory is provided in Eq. (17). From Eq. (15), the new instantaneous frequency estimation can not only adapt to the "small" frequency modulation, i.e., the case of $c = \phi''(t) = 0$, but also accommodate to strong frequency modulation, i.e., the case of $c = \phi''(t) \neq 0$. In short, ASET as an improved version of SET, it not only can deal with a signal with "small" frequency modulation but also can accommodate to the strong frequency modulation signal. Moreover, a high order version of synchroextracting transform is also possible for ASET, while their analysis is similar. Simulated experimental studies and rotating machine vibration signal would be applied to validate the effectiveness of ASET in Section 4 and Section 5.

4. Numerical experiments and performance exploration

To investigate the performance of the proposed ASET approach, a simulation study is used to demonstrate its effectiveness, embracing Rényi entropy to measure the sharpness of TFR, the ability of signal reconstruction and robustness to noise pollution. The comparison is made between several traditional and recently introduced TFA methods, i.e., the STFT, SST, RM, and SET. Noted in this simulation, it is necessary to choose the suitable window function to calculate the result of STFT. Meanwhile, considering the Gaussian window function has the minimal area of the Heisenberg box [13], so the Gaussian window is used as,

$$g(t) = e^{-\pi\cdot t^2\frac{1}{0.32^2}} \tag{20}$$

4.1. Mono-component signal

To achieve a quantitative analysis between the various methods, a mono-component signal is used for comparison first. The signal is modeled as

$$x(t) = e^{(t-0.5)^2}\cdot\sin(2\pi\cdot(50t + 2.0\cdot\sin(2\pi 1.3\cdot t))) \tag{21}$$

The mono-component signal $x(t)$ is an amplitude modulation (AM) and frequency modulation (FM) signal, with varying amplitude and strong nonlinear sinusoidal frequency modulations. It is sampled

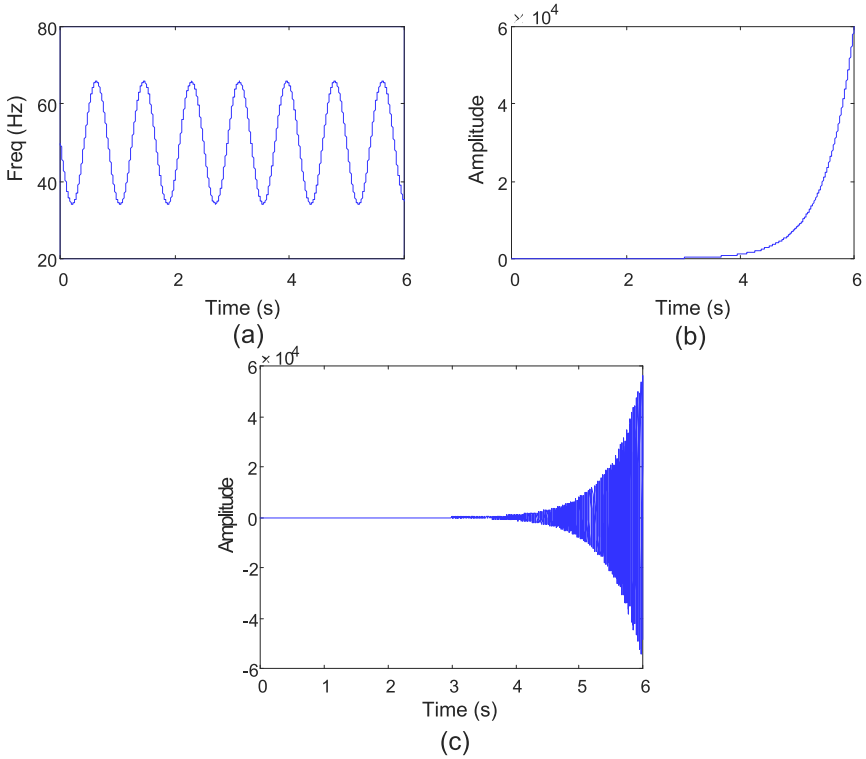

Fig. 3. Mono-component signal $x(t)$, (a) IF trajectory, (b) IA trajectory, (c) Waveform of $x(t)$.

with 1024 Hz. For the signal model defined in Eq. (21), its IF trajectories are plotted in Fig. 3(a). The corresponding instantaneous amplitude (IA) trajectory and waveform are generated in Fig. 3(b) and Fig. 3(c).

(a) Qualitative evaluation the sharpness of TFR

To explore the performance to noise influence of different TFAs, white Gaussian noise is added into the simulated signal (signal-to-noise ratio (SNR) is 5 dB). The noise-free and noise-contaminated signal is analyzed by ASET and other TFA methods, namely STFT, SST, SET and RM.

In Figs. 4 and 5, the TFRs for both noise free and noise contaminated signal are depicted. In the noise free case, it can be observed that the TFRs obtained by STFT, SST and SET (shown in Fig. 4(A)–(C)) have a low energy concentration representation. Furthermore, it is more clear in the specific region ([1.10,1.35]s × [35]Hz shown in Fig. 4(a)–(c)), i.e., the zoomed rectangular region of corresponding Fig. 4(A)–(C). It means that these methods fail to represent the TF content of the simulated signal $x(t)$ properly. Similarly, in the noise contaminated case, for SST result (in Fig. 5(B) and zoomed version (b)), it is smeared, since the SST squeezes the TF coefficients only in the frequency direction. Due to RM is a reassigned but irreversible TFA method, it reassigns the TF spectrogram in the two-dimensional TF directions. Thus, it has a slight enhancement for the sharpness of the spectrogram (shown in Fig. 4, 5(D)

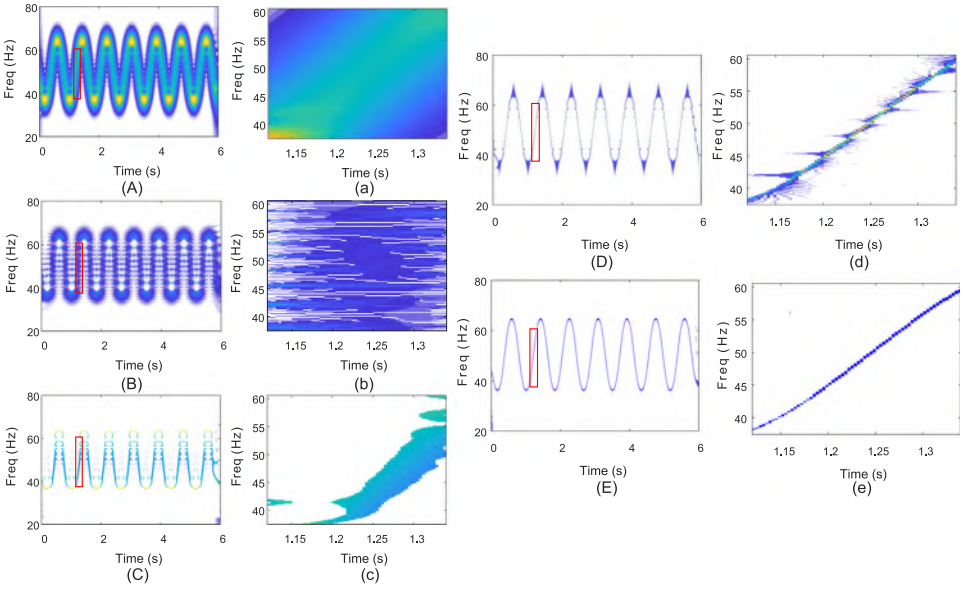

Fig. 4. TFRs of free noisy signal $x(t)$ obtained by (A) STFT, (a) zoomed version of STFT, (B) SST, (b) zoomed version of SST, (C) SET, (c) zoomed version of SET, (D) RM, (d) zoomed version of RM, (E) ASET, (e) zoomed version of ASET.

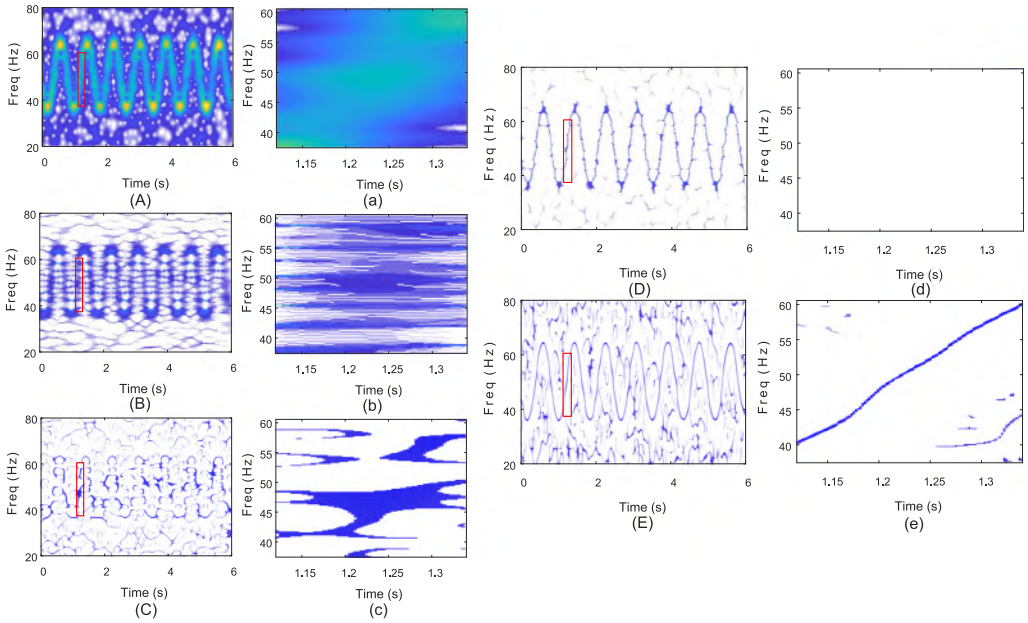

Fig. 5. TFRs of noisy signal $x(t)$ with SNR = 5 dB obtained by (A) STFT, (a) zoomed version of STFT, (B) SST, (b) zoomed version of SST, (C) SET, (c) zoomed version of SET, (D) RM, (d) zoomed version of RM, (E) ASET, (e) zoomed version of ASET.

and (d)). Clearly, the results of ASET (in Fig. 4, 5(E) and (e)) are better than the other methods.

(b) Quantitative comparison the sharpness of TFR

To quantitatively evaluate the energy concentration performance of different methods, the Rényi entropy [33,34] is employed to evaluate the performance of difference TFA methods in this paper. The Rényi entropy of order α for a continuous-valued bivariate density $P(x,y)$ can be measured as follows,

$$R_P^{\alpha} = \frac{1}{1-\alpha}\log_2 \frac{\iint P^{\alpha}(x,y)dxdy}{\iint P(x,y)dxdy} \tag{22}$$

For a signal whose TFR is $P(t,\omega)$, and the Rényi entropy is defined as a prenormalized version equivalent to normalizing the signal energy before raising the TFR to the α power

$$R_P^{\alpha} = \frac{1}{1-\alpha}\log_2 \iint \left(\frac{P(t,\omega)}{\iint P(t,\omega)dtd\omega}\right)^{\alpha} dtd\omega \tag{23}$$

From [34], it proved that a lower Rényi entropy value denotes a more energy concentrated TFR. And the third-order Rényi entropy is used to quantitatively evaluate the TF energy concentration since it has been proved that $\alpha = 3$ is the smallest integer value to yield a well-defined useful information evaluation for a large class of signals [34]. The corresponding Rényi entropies are listed in Table 2. From Table 2, it can be observed that ASET has the lowest Rényi entropy, which means that it can generate the more energy concentrated TFR among five methods, see Fig. 4(E) and (e). In this case, it can be found that the TF energy concentration is greatly improved by ASET which measured the lowest Rényi entropy, see Fig. 6(a). Compared with other methods, ASET result can almost perfectly characterize the fast time varying feature, the result is almost identical to the ideal TF spectrogram in Fig. 3(a). It may conclude that the proposed ASET can effectively improve TF energy concentration through the comparison among above five TFA methods.

(c) Evaluation the robustness to noise interference

In order further to visualize the influence of noise, different level noises (SNR from 0 to 30 dB) are added into the original $x(t)$ signal. A comparison of Rényi entropy value under different noise levels are made in Fig. 6(a). It indicates that with the increase of noise, the value of Rényi entropy increases. It means that the energy concentration of TFR degrades. While, ASET exhibit the best ability of energy concentration with the minimal Rényi entropy, and its result can be seen in Fig. 6(a). Thus, based on the above discussion, it may conclude that for the mono-component signal with fast and strong frequency modulation, the ASET not only can enhance the TF energy concentration but also can improve the robustness to noise influence.

4.2. Multicomponent signal

In this section, we consider a multicomponent signal consisting of three different frequency modulated components. In this case, the simulated multicomponent signal is used to explore the performance of the proposed method ASET comparing with five traditional TFA methods. The signal $y(t)$ are written as,

$$y(t) = \begin{cases} y_1(t) = \sin(2\pi \cdot (10t + 2.0 \cdot \cos(2\pi \cdot 0.3t))) \\ y_2(t) = \sin(2\pi \cdot (30t + 1.5 \cdot \cos(2\pi \cdot 0.8t))) \\ y_3(t) = \sin(2\pi \cdot (60t + 4.0 \cdot \cos(2\pi \cdot 0.8t))) \end{cases} \tag{24}$$

Eq. (24) tells that signal $y(t) = y_1(t) + y_2(t) + y_3(t)$ in which three types of nonlinear sinusoidal frequency modulations are included. The first component has a very slow varying sinusoidal frequency modulation. And the fast and strongly sinusoidal frequency modulation is contained in the other two components. The simulated signal is sampled with 1024 Hz. The ideal IF trajectory and waveform can correspondingly be drawn in Fig. 7(a) and (b). Furthermore, it can be observed that the components of $y_2(t)$ and $y_3(t)$ have a trend of distinct fast-varying frequency modulation.

Similarly, as analyzing of the mono-component signal $x(t)$, in this section, the multicomponent signal $y(t)$ is used to explore the performance of TFR, the ability of reconstructed signal, the robustness to noise pollution, the performance of extracted TF ridges and comparisons of computational time.

(a) Qualitative evaluation the TF energy concentration

Fig. 8 and 9 present the TFRs including noise free and noise contaminated (SNR = 5 dB) cases. In the noise free case, the component $y_1(t)$ (see in Fig. 7(a)) consists of the very slow frequency modulation, thus SET and RM can characterize this slow time-varying feature properly, see in Fig. 8(c) and (d). However, owing to the component of $y_3(t)$ including a fast and strong time-varying frequency modulation, apart from RM has a slight improvement for

Table 2
Rényi entropy of different TFA methods for $x(t)$ (with SNR = 5 dB)

TFA methods	STFT	SST	SET	RM	ASET
Rényi entropy	18.52	16.98	15.20	14.90	13.19

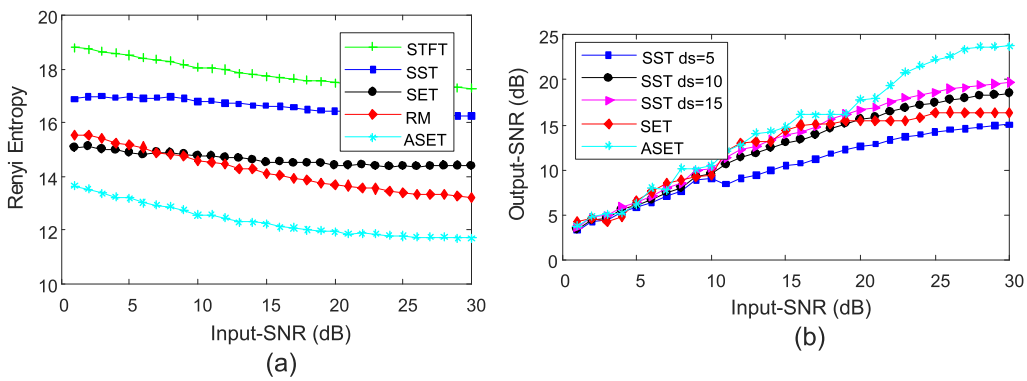

Fig. 6. (a) Rényi entropies of the different TFRs for signal $x(t)$ with different noise levels from 0 to 30 dB. (b) The SNR of reconstructed results by different TFA methods with different noise levels from 0 to 30 dB.

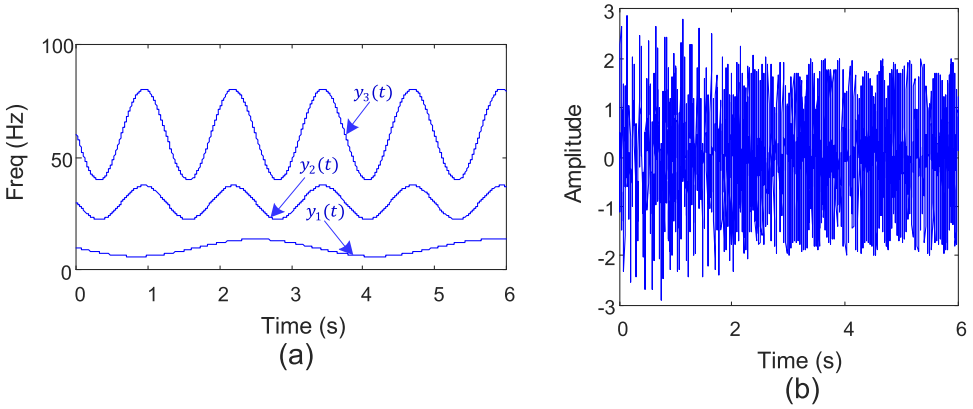

Fig. 7. (a) Ideal TF trajectory (b) Waveform of $y(t)$.

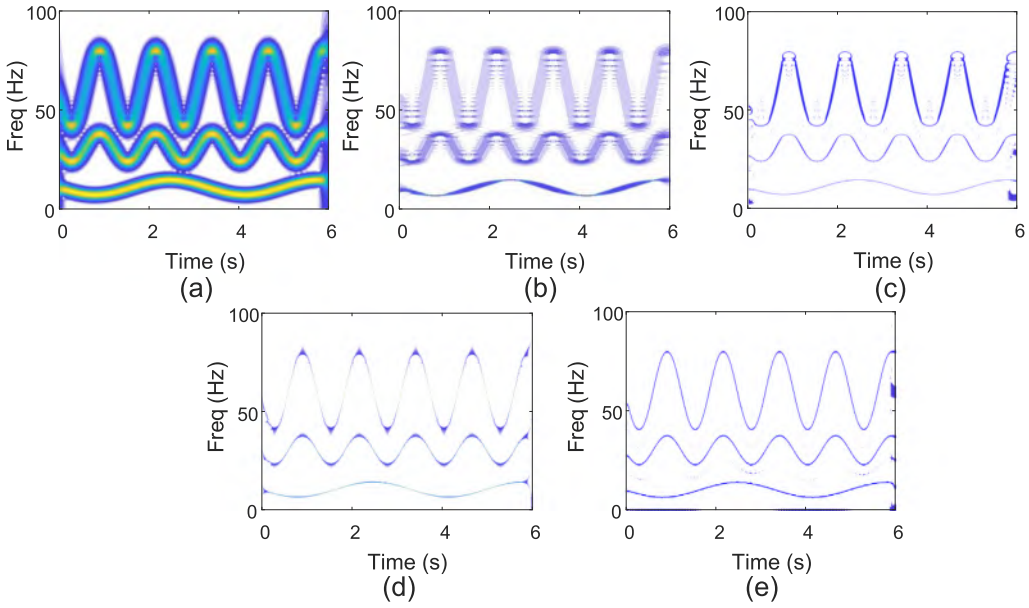

Fig. 8. TFRs of free noisy signal $y(t)$ obtained by (a) STFT, (b) SST, (c) SET, (d) RM, (e) ASET.

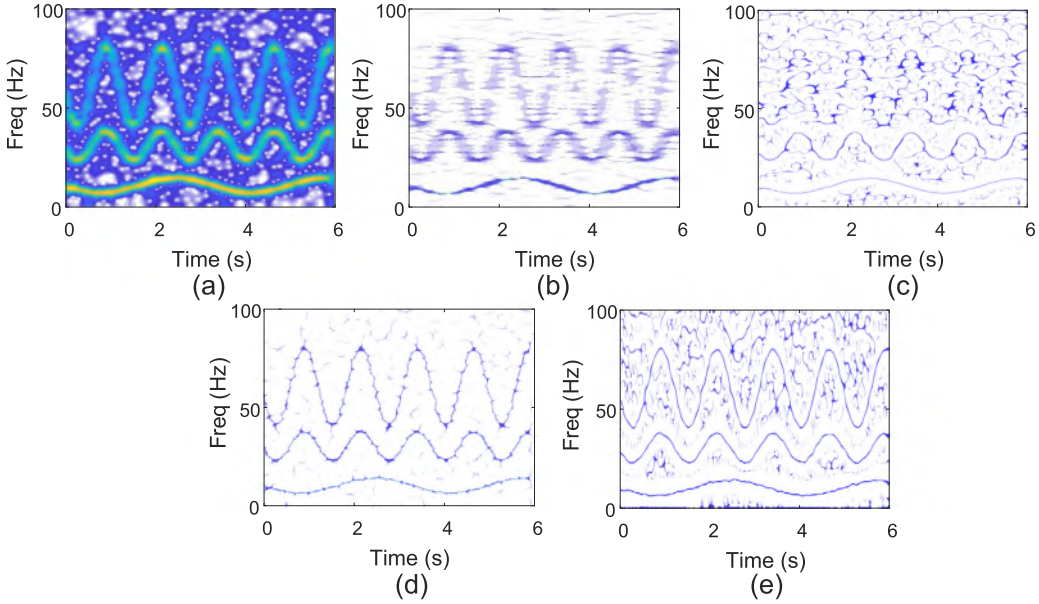

Fig. 9. TFRs of noisy signal $y(t)$ with SNR = 5 dB obtained by (a) STFT, (b) SST, (c) SET, (d) RM, (e) ASET.

TFR (shown in Fig. 8(d)), STFT, SST and SET cannot appropriately describe the TF feature, see in Fig. 8(a)–(c). Similarly, in the noise contaminated case, STFT and SST also have a smeared TFR (see in Fig. 9(a) and (b)). Fortunately, ASET can appropriately describe TF content of signal $y(t)$ under both noise free and noise contaminated conditions, see in Fig. 8, 9(e).

(b) Quantitative analysis the TF energy concentration

To quantitative analysis the TF energy concentration, the Rényi entropy is again used to measure the performance among these five methods. The corresponding Rényi entropies are listed in Table 3. In Table 3, it can be seen that ASET also has the lowest Rényi entropy, and it means that it has a better ability for TFR among the five methods. In this case, it also can be found that the sharpness of the TF spectrum is substantially enhanced by ASET, see in Fig. 8, 9(e). Compared with other methods, ASET features prominent advantages in TFR, the result (see in Fig. 8, 9(e)) is almost identical to the ideal TF spectrogram in Fig. 7(a).

(c) Evaluation of interested signal reconstruction performance

Regarding evaluate the signal reconstruction performance, as it noted that in [11,13], SST and SET have main advantage over RM is its ability to reconstruct signal. Therefore, reconstruction interested signal performance of ASET is compared with SST and SET. The simulated signal in Eq. (21) and Eq. (24) are also added noises (noise levels from 0 to 30 dB). From the signal reconstruction formula in Eq. (6) and Eq. (19), it tells that SET and ASET, to reconstruct a signal, all need one parameter $\omega_{ins}(t,f)$, i.e., the IF trajectory corresponding to each component.

For the mono-component signal, the IF trajectory can be estimated by the maximum value detection method directly, i.e., $\omega_{ins}(t,f) = arg\ max_{\omega}|TFR(t,f)|$, where $TFR(t,f)$ denotes the TFA to be analyzed. But for SST, apart from the parameter of $\omega_{ins}(t,f)$, it also needs to know the integration parameter *ds* which is utilized to measure the integration region [13]. So, three different integration parameters, ds = 5,10,15 are used to reconstruct the component of original signal.

However, for the multicomponent signal, the first step is to decompose each mono-component in a multicomponent signal and then is to estimate each corresponding IF trajectories. Fortunately, a new algorithm has been introduced in [35], which is used to detect all IF trajectories at the same time. Hence, if the number of K is known, this algorithm can be used to calculate the local minimum value of the function

$$E(\phi) = \sum_{k=1}^{K} - \int_{-\infty}^{+\infty} |TFR(t,\phi_k(t))|^2 dt + \int_{-\infty}^{+\infty} \left(\lambda \cdot \phi_k'(t)^2 + \beta \cdot \phi_k(t)^2\right) dt \tag{25}$$

where $\sum_{k=1}^{K}(t,\phi_k(t))$ denotes the detection of the IF trajectories, λ, β are two parameters to adjust the level of regularization. For the multicomponent signal $y(t)$ in Eq. (24), the parameter of K can be set as 3.

So, the results of mono-component signal $x(t)$ and multicomponent signal $y(t)$ are displayed in Figs. 6(b) and 10(b). For the reconstruction of signal $x(t)$, it can be seen that, for SST method, more TF coefficients such as ds = 15 yield better robustness to noise. For SNR from 1 dB to 18 dB, apart from STFT, all these TFAs have a similar performance. For ASET, owing to the introduction of second-order approximation, it has an excellent performance of signal reconstruction as it is shown in Fig. 6(b). Moreover, for multicomponent signal $y(t)$ it also indicates that ASET provides competitive advantage than other TFAs (see in Fig. 10(b)). And looking at results (shown in Figs. 11 and 12) for each mono-component, one observes that for $y_1(t)$ component since it is a slight modulated, the corresponding TF ridges can be precisely detected among the three methods SST, AET and ASET in low (SNR = 5 dB) or high (SNR = 20 dB) SNR conditions. However, owning the component $y_3(t)$ which contains strong nonlinear frequency modulations, both SST and SET (see in Figs. 11(a), (b) and 12(a), (b)) fail to represent the components as the ideal energy concentrated TF trajectories, some important TF information being spread out around the trajectories. Fortunately, when the second -order local instantaneous frequency approximation terms was considered in the definition of ASET, it not only can enhance the quality of interested signal component reconstruction but also the trajectories detection. To further evaluate the extracted time-frequency trajectory, an error between ideal trajectory and estimated trajectory can be measured by an indicator such as mean absolute error (MAE), which is calculated as

$$MAE = \frac{1}{K}\sum_{k=1}^{K}\left|\frac{IF_e(k) - IF_i(k)}{IF_i(k)}\right| \tag{26}$$

where $IF_e(k)$ is the extracted time-frequency trajectory by time-frequency representation methods and $IF_i(k)$ is ideal

Table 3
Rényi entropy of different TFA methods for $y(t)$ (with SNR = 5 dB)

TFA methods	STFT	SST	SET	RM	ASET
Rényi entropy	18.4	16.38	14.74	14.81	13.55

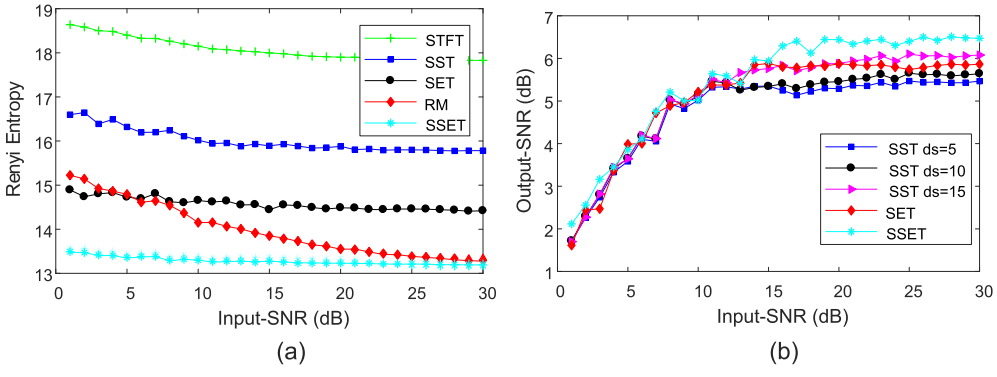

Fig. 10. (a) Rényi entropies of the different TFRs for signal $y(t)$ with different noise levels from 0 to 30 dB. (b) The SNR of reconstructed results by different TFA methods with different noise levels from 0 to 30 dB.

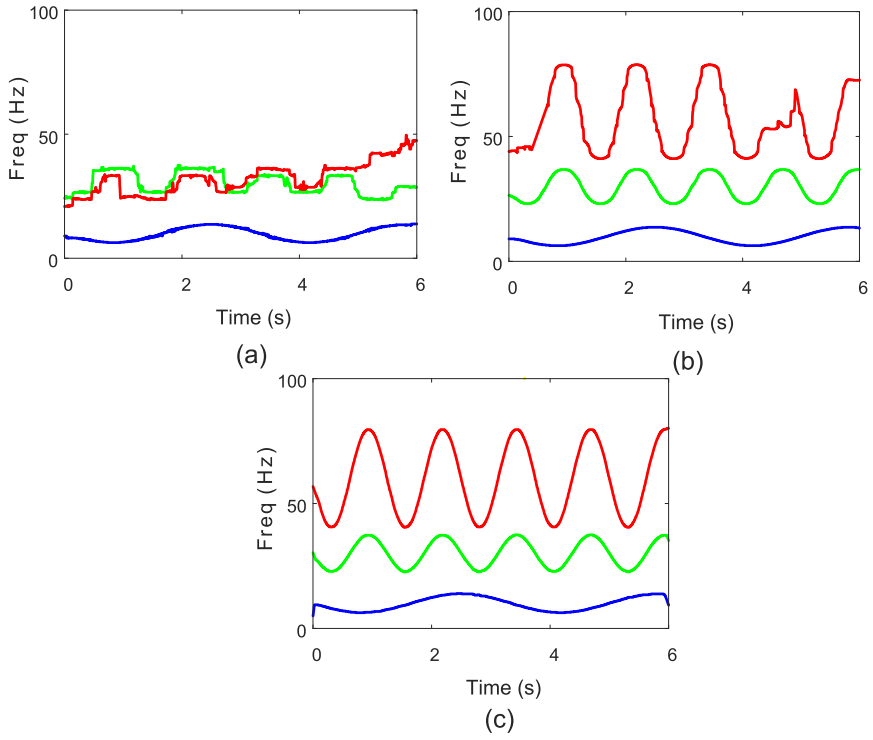

Fig. 11. SNR added to the signal is 20 dB, and Ridges estimated by (a) SST, (b) SET, (c) ASET.

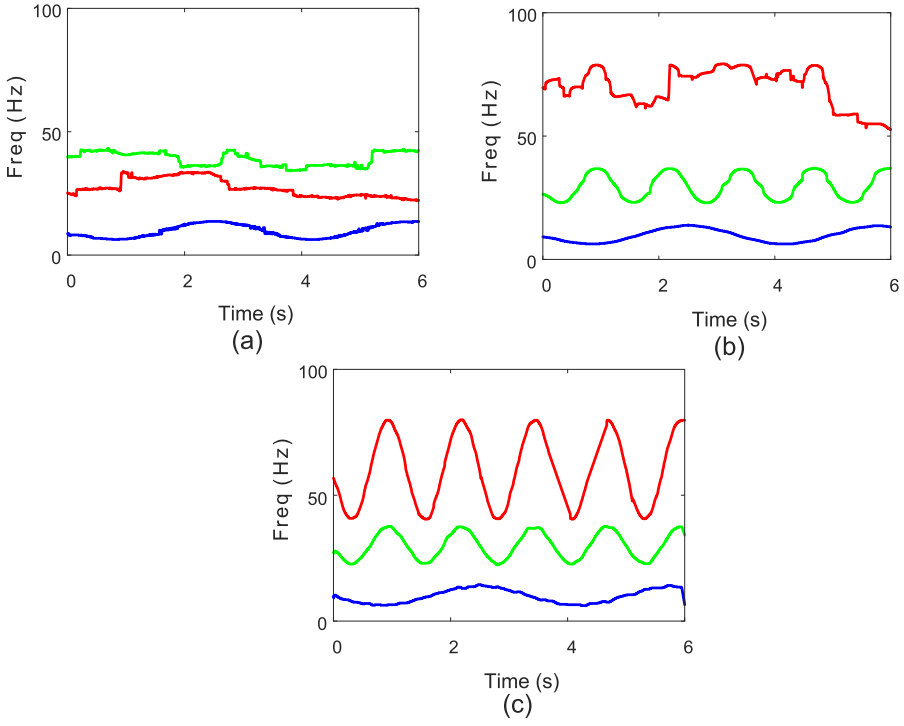

Fig. 12. SNR added to the signal is 5 dB, and Ridges estimated by (a) SST, (b) SET, (c) ASET.

time-frequency trajectory. For the extracted time-frequency trajectory shown in Figs. 11 and 12, and the values of MAE are calculated as 0.683, 0.362, 0.002 and 0.894, 0.435, 0.034 respectively.

(d) Evaluation the robustness to noise pollution

Similarly to the mono-component signal $x(t)$ analysis, different level noises (SNR from 0 to 30 dB) are also added into the original $y(t)$ signal. Another comparison of Rényi entropy value under different noise levels are made in Fig. 10(a). It also shows that ASET exhibit the best ability of energy concentration among the other five methods. Thus, for the multicomponent signal, ASET again features advantages in improving the sharpness of the TF spectrum and can enhance the robustness to noise pollution.

(e) Evaluation of extracting TF ridges

To investigate the ability of detection of TF ridges for multicomponent signal under different levels of noise pollution. Figs. 11 and 12 (SNR of signal are 20 dB and 5 dB, receptively) illustrate the

corresponding plots of estimated ridges. The time-varying feature components of $y_2(t)$ and $y_3(t)$ in the SST results (see in Figs. 11 (a) and 12(a)) are heavily affected by noise. Owning to component of $y_3(t)$ including the fast and strong frequency modulation, the analysis results of SST and SET (see in Figs. 11, 12(a) and (b)) fail to describe this TF content under different noisy levels. However, for the above different noise levels, ASET (see in Figs. 11(c) and 12(c)) can always estimate the TF ridges which is almost identical to the ideal TF. Thus, it indicated that ASET is a better choice for TF ridge detection.

(f) Comparisons of computational time

The computational efficiency of time-frequency analysis (TFA) methods is vital for practice implementation. In this case, software for implementing the above methods is MATLAB (version 2018a).

Table 4
Required computation time

TFA methods	STFT	SST	SET	RM	ASET
Time(s)	0.020	0.060	0.049	0.052	0.042

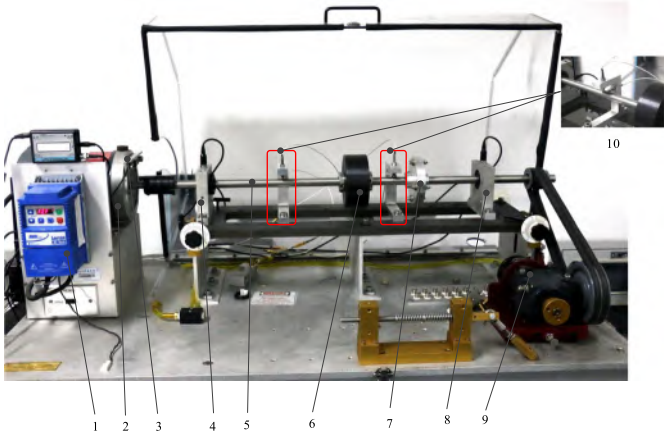

Fig. 13. Experimental set-up of case A: 1-motor controller, 2-drive motor, 3-tachometer,4,8-bearing pedestals 5-rotor 6-disk, 7-mating flanges 9-gearbox 10-zoomed proximity probes.

These methods are run on a machine utilizing a 12-core CPU (Intel i7 8700 K) with 32G of DDR4 memory, and the required computational time for the aforementioned five kinds of TFA methods are listed in Table 4.

5. Application in rotating machine vibration signal analysis

5.1. Case A

So far, all the examples have focused on the simulated signal. In this section, the experimental signal measured from a real test rig is utilized to validate the capability of ASET. A machinery fault simulator-magnum (MFS-MG) at University of Electronic Science and Technology of China (UESTC), Engineering Reliability and Prognostic and Health Management Laboratory (ERPHM) is used for the study. The experimental set-up consists of a drive motor which is a 2.24 kW three-phase electrical motor controlled by a motor speed controller. An accelerometer (with a sensitivity of 100 mV/g and frequency range 0–10 kHz, see in Fig. 13, and a shaft tachometer (produced by Encoder Products Co. with 1 pulse/revolution) are used for capturing vibration and Tacho signals simultaneously. During the experiments, the data are captured by accelerometers mounted to bearing pedestals (see in Fig. 13 (4, 8)) under fluctuating speed from 10 Hz to 40 Hz within 20 s and 12 s data is used for the following analysis. The sampling frequency is set to be 10,240 Hz. The whole set-up arrangement is shown in Fig. 13. Meanwhile, the instantaneous speed of the motor is recorded by a tachometer and the collect the tacho signal is plotted in Fig. 14(c), with which IF can be calculated for comparison.

To investigate the performance of ASET applied in rotating machine vibration signal, the measured signal by an accelerometer mounted on bearing pedestals (see in Fig. 13-4) is used for analyzing. The waveform of the raw vibration signal and its frequency spectrum is displayed in Fig. 14(a) and (b), respectively. According to the measured tacho signal shown in Fig. 14(c), the instantaneous rotating frequency of the rotor shaft can be estimated in Fig. 14(d). Fig. 15 shows the corresponding time-frequency representations (TFRs) associated with the five different methods, as well as zoomed-in the region at ([1.50,3.50]s × [10]) Hz shown in Fig. 15 (a–e), i.e., the zoomed-in rectangular region in Fig. 15(A–E). From

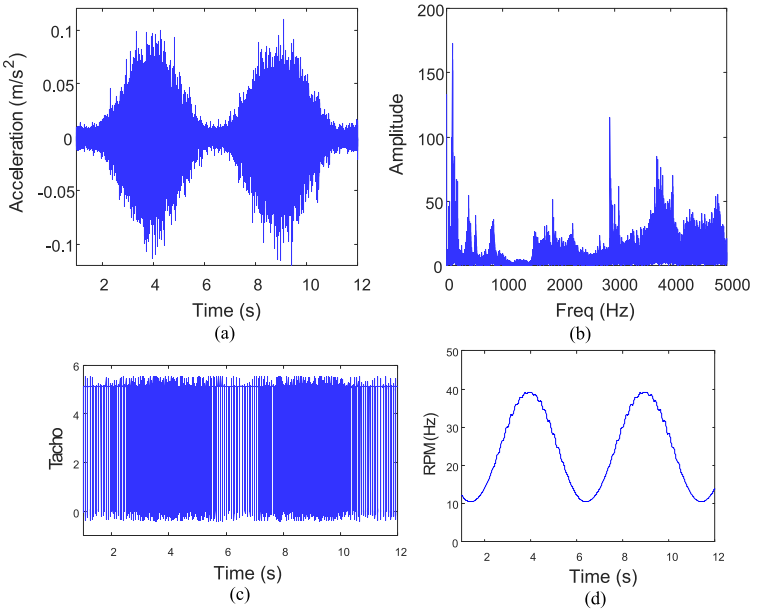

Fig. 14. (a) Waveform of vibration signal (b) spectrum of vibration signal (c) tacho signal (d) rotating frequency measured by tachometer.

the result of ASET shown in Fig. 15(E) and (e), the energy of TFR is concentrated along the ridge, whereas in the case of STFT, SST and SET (see in Fig. 15(A, a), (B, b) and (C, c)) they fail to provide accuracy time-frequency representations. According to the results of Fig. 15(E) and (e), ASET clearly features advantages for TFR under fluctuated rotational speed condition. Apart from ASET, all the other methods cannot give a satisfied result for characterizing of signals under fluctuated rotational speed condition.

Utilizing the IF trajectory estimated by ASET, the extracted IF ridge is depicted in Fig. 16(a). From Fig. 16(b), it can be observed that instantaneous rotating frequency measured by ASET result almost perfectly match the estimated result of the tacho signal. Furthermore, the error between them can be measured by an indicator like MAE, which is defined in Eq. (26). In this real mechanical vibration signal case, the MAE value is almost 0.0007, and it clearly interprets that ASET can accurately reflect instantaneous rotating speed fluctuation of the vibration signal. Therefore, ASET has a competitive advantage to characterize the features of the frequency modulated signal. In the case of signal reconstruction, the comparison between the original vibration and reconstructed signal (the blue solid line is the original vibration signal and the red dotted line is the reconstructed signal) are shown in Fig. 17(b). The error between the reconstructed signal and the original signal can also be measured by an indicator such as root mean square error (RMSE), and it can be calculated as,

$$RMSE = \sqrt{\frac{1}{K}\sum_{k=1}^{K}(sig_r(k) - sig_o(k))^2} \tag{27}$$

where $sig_r(k)$ is the reconstructed signal and $sig_o(k)$is the original vibration signal. In this experimental vibration signal analysis case, RMSE value is almost 0.003, which convinced that the proposed ASET method has excellent reconstruction ability.

5.2. Case B

Compared with case A in Section 5.1, to investigate the performance of proposed ASET further studied in terms of the influences from harmonics, a real experimental study is constructed and result is discussed in case B. An experimental rotor-bearing system test rig (see in Fig. 18) is used to measure vibration signal for analysis. With assembling of an extra disk and a shaft axis adjustment device shown in Fig. 18, harmonics can be introduced to the measured signal. In this case, signals are measured by two proximity probes which are mounted on each bearing housing in the vertical and horizontal directions under fluctuating operational conditions with 20 s. For analysis, 8 s data is used. Besides, to reduce the influence between these two probes, their positions have an offset with 90 degrees as illustrated in Fig. 18 (proximity probes). The time-domain wave is depicted in Fig. 19.

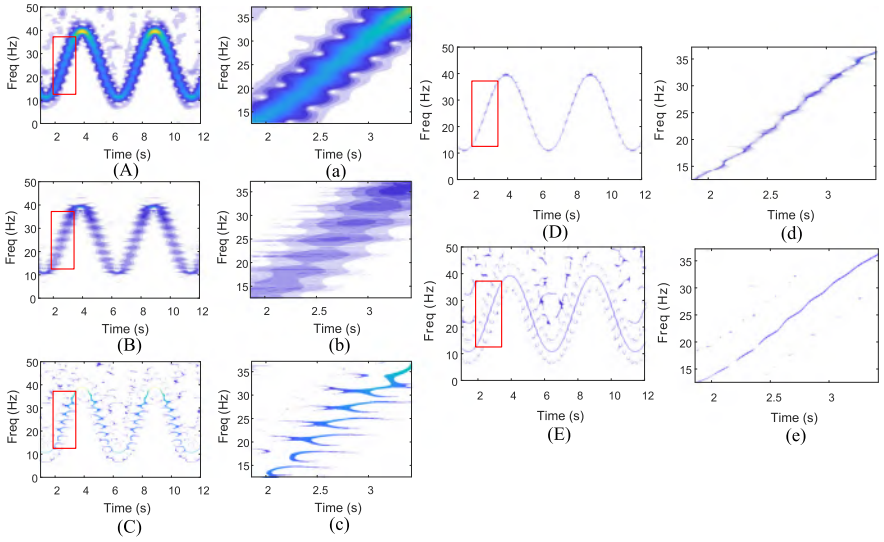

Fig. 15. TFRs of vibration signal achieved by (A) STFT, (a) zoomed version of STFT , (B) SST, (b) zoomed version of SST, (C) SET, (c) zoomed version of SET, (D) RM, (d) zoomed version of RM, (E) ASET, (e) zoomed version of ASET.

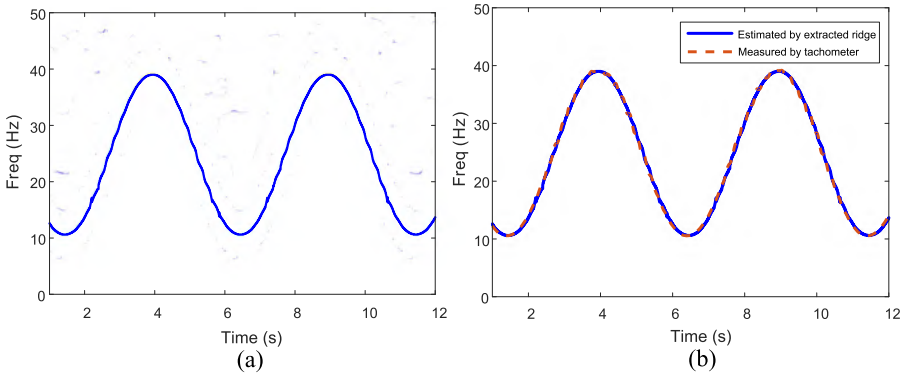

Fig. 16. (a) Extracted TF ridge (b) Instantaneous rotating frequency measured by extracted ridge and tachometer.

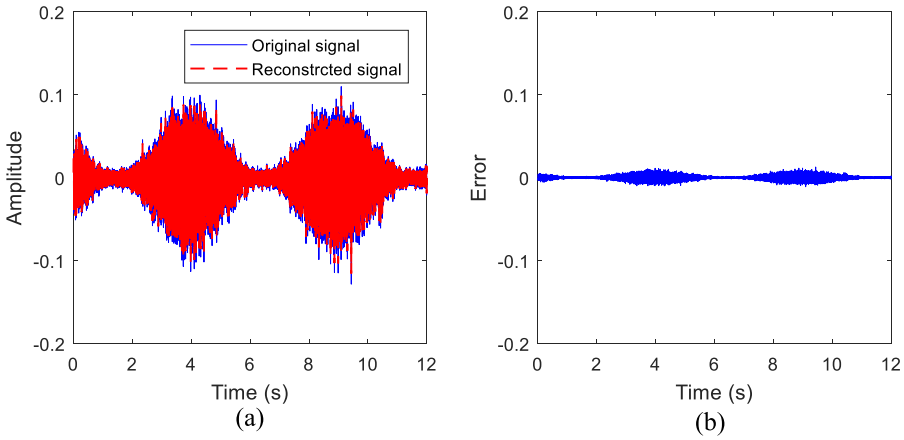

Fig. 17. (a) The comparison between the original vibration and reconstructed signal (b) The corresponding residuals after subtracting the original vibration signal.

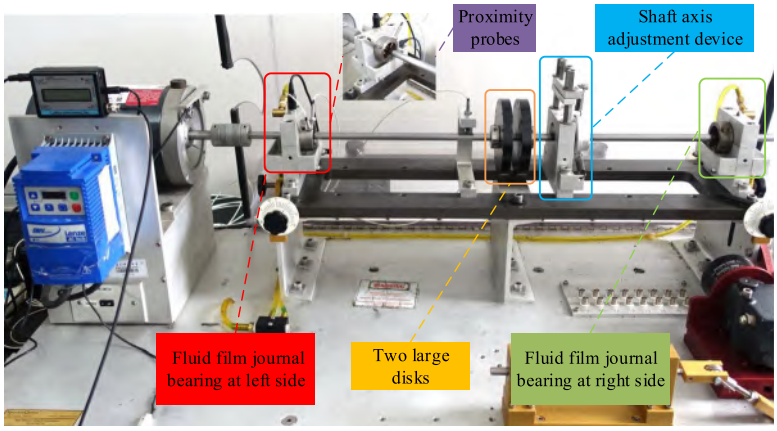

Fig. 18. Experimental set-up of case B.

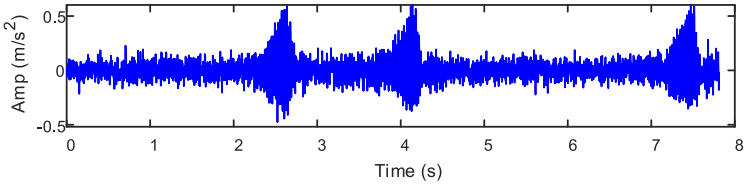

Fig. 19. Waveform of harmonic vibration signal.

The TFRs associated with five different methods, as well as zoomed-in region at ([4.8, 6.2]s×[18.9, 93.2]Hz) are shown in Fig. 20(a–e), i.e. the zoomed-in rectangular region in Fig. 20(A–E). From the result of ASET, it can be seen that the energy of TFR is concentrated along the ridge (see in Fig. 20(e)). For the other methods such as STFT, SST, RM and SET (see in Fig. 20(A, a), (B,b), (C,c) and (D,d)), however they cannot provide a concentrated time-frequency representations. Especially for the 2nd harmonic signal, these methods almost completely fail to obtain an accurate TFR. It demonstrated that the proposed ASET, indeed, features advantages in TFR under fluctuating operational conditions. Apart from ASET, the other methods mentioned above fail to provide a satisfactory result for characterizing of the 1st and 2nd harmonics signal. The estimated IF trajectories are depicted in Fig. 21, and it can be seen that only ASET can obtain well concentrated and separated time-frequency representation. Specifically, SST and SET fail to estimate the ridge of the 2nd harmonic component and it may attribute the variation of the frequency range of the 2nd harmonic component is wider than the 1st harmonic component. Moreover, together with noise pollution in a real operational environment (in Fig. 19), it also makes the extraction of IF trajectories are even more challenging. Finally, the indicator of MAE is again used to evaluate the signal reconstruction ability, and the MAE value is calculated to be 0.0006 based on Eq. (26). The comparison between the measured signal and reconstructed signal (blue solid line is denoted as a signal with harmonics and the red solid line is the reconstructed signal) are depicted in Fig. 22. The error between the reconstructed signal and harmonics signal can also be measured by RMSE (in Eq. (27)) and its value is 0.025. In short, the proposed ASET exhibits a competitive advantage to represent the measured signal with harmonics under fluctuating operational conditions.

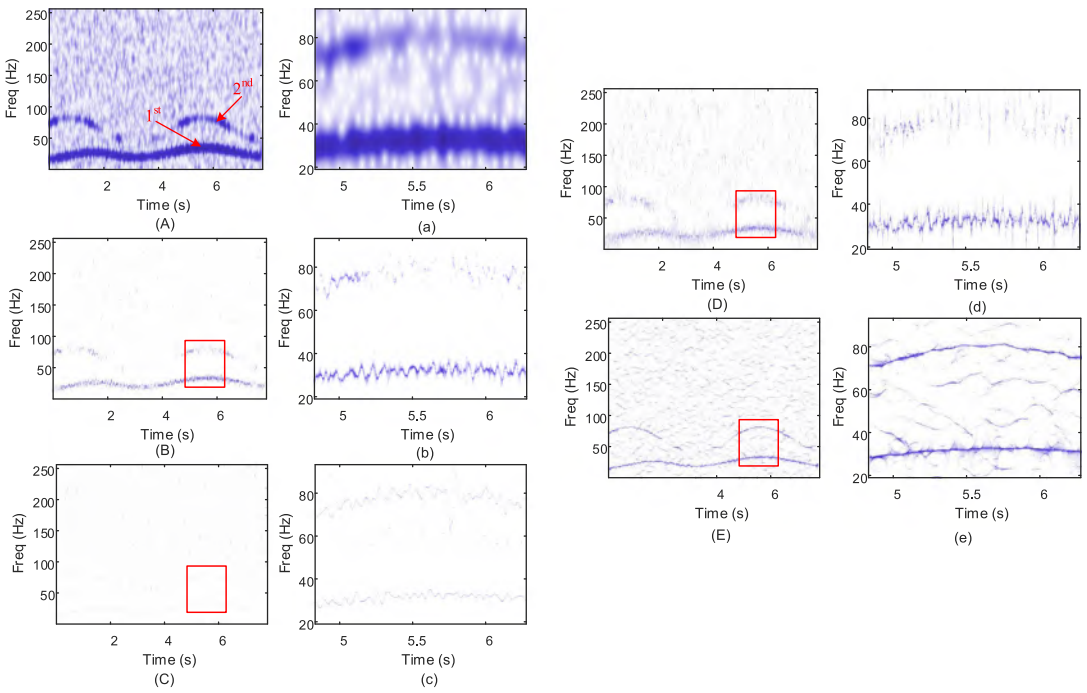

Fig. 20. TFRs of harmonic vibration signal achieved by (A) STFT, (a) zoomed version of STFT , (B) SST, (b) zoomed version of SST, (C) SET, (c) zoomed version of SET, (D) RM, (d) zoomed version of RM, (E) ASET, (e) zoomed version of ASET.

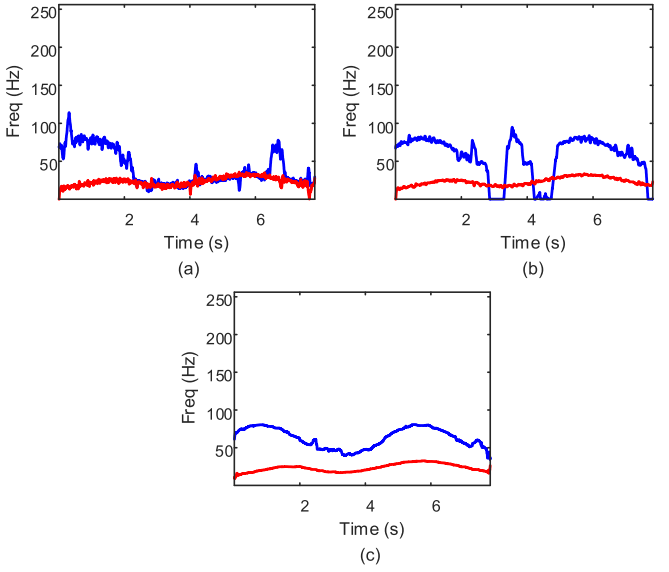

Fig. 21. Ridges estimated by (a) SST, (b) SET, (c) ASET.

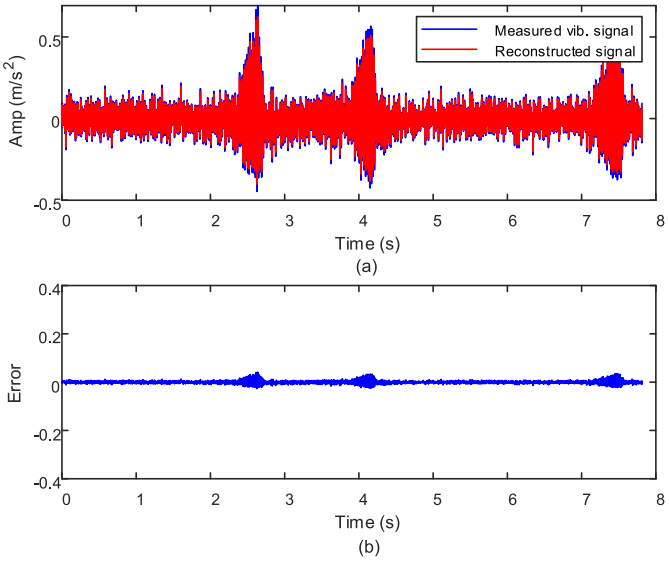

Fig. 22. (a) The comparison between the harmonic vibration signal and reconstructed signal (b) The corresponding residuals after subtracting the harmonic vibration signal.

6. Conclusion

In this paper, ameliorated synchroextracting transform (ASET) can circumvent the drawbacks of the standard SET and reassigned transformation. In the ASET, based on the utilizing the second-order Taylor expansion to estimate signal local IF, the time and frequency variables can be simultaneously considered to overcome the diffusion limitation of the SET for the signal with fast and strong time-varying IF and meanwhile remain reconstruction ability. Indeed, it is emphasized that ASET can be viewed as an upgraded version of the post-processing TFA method, while it holds the strategy of synchroextracting manner, allowing for a better reconstruction by a direct and convenient step. All the simulation and real mechanical vibration signal studies suggest that ASET is a competitive method for the TF representation, signal reconstruction, and better robustness to noise pollution.

Declaration of Competing Interest

The authors declared that there is no conflict of interest.

Acknowledgments

This research is supported by the National Key Research and Development Program of China (Project No. 2017YFC0108401 and 2018YFB1702400), Fundamental Research Funds for the

Centered University (ZYGX2016J111), National Natural Science Foundation of China (51305067), and the Natural Sciences and Engineering Research Council of Canada (Grant #RGPIN-2015-04897).

References

[1] C. Tantibundhit, F. Pernkopf, G. Kubin, Joint time–frequency segmentation algorithm for transient speech decomposition and speech enhancement, IEEE Trans. Audio Speech Lang. Process. 18 (2010) 1417–1428.

[2] K. Wang, P.S. Heyns, Application of computed order tracking, vold–kalman filtering and emd in rotating machine vibration, Mech. Syst. Signal Process. 25 (2011) 416–430.

[3] C.L. Herry, M. Frasch, A.J. Seely, H.-T. Wu, Heart beat classification from single-lead ecg using the synchrosqueezing transform, Physiol. Meas. 38 (2017) 171.

[4] P. Chen, K. Wang, K. Feng, Application of order-tracking holospectrum to cracked rotor fault diagnostics under nonstationary conditions, in: Prognostics and System Health Management Conference (PHM-Chengdu), 2016, IEEE, pp. 1–6.

[5] H.S. Black, Modulation theory, van Nostrand, 1953.

[6] E. Wigner, On the quantum correction for thermodynamic equilibrium, Phys. Rev. 40 (1932) 749.

[7] A. Lefebvre, T. Corpetti, L.H. Moy, Estimation of the orientation of textured patterns via wavelet analysis, Pattern Recogn. Lett. 32 (2011) 190–196.

[8] J.H. Lee, J. Kim, H.J. Kim, development of enhanced wigner-ville distribution function, Mech. Syst. Signal Process. 15 (2001) 367–398.

[9] S. Mallat, A Wavelet Tour of Signal Processing, Academic Press, 1999.

[10] K. Kodera, R. Gendrin, C. Villedary, Analysis of time-varying signals with small bt values, IEEE Trans. Acoust. Speech Signal Process. 26 (1978) 64–76.

[11] I. Daubechies, J. Lu, H.-T. Wu, Synchrosqueezed wavelet transforms: an empirical mode decomposition-like tool, Appl. Comput. Harmonic Anal. 30 (2011) 243–261.

[12] G. Thakur, E. Brevdo, N.S. Fučkar, H.-T. Wu, The synchrosqueezing algorithm for time-varying spectral analysis: robustness properties and new paleoclimate applications, Signal Process. 93 (2013) 1079–1094.

[13] G. Yu, M. Yu, C. Xu, Synchroextracting transform, IEEE Trans. Industr. Electron. 64 (2017) 8042–8054.

[14] S. Wang, X. Chen, C. Tong, Z. Zhao, Matching synchrosqueezing wavelet transform and application to aeroengine vibration monitoring, IEEE Trans. Instrum. Meas. 66 (2017) 360–372.

[15] D. Iatsenko, P.V. McClintock, A. Stefanovska, Linear and synchrosqueezed time-frequency representations revisited: overview, standards of use, resolution, reconstruction, concentration, and algorithms, Dig. Signal Process. 42 (2015) 1–26.

[16] D. Iatsenko, P.V.E. Mcclintock, A. Stefanovska, Linear and synchrosqueezed time-frequency representations revisited. Part I: Overview, standards of use, related issues and algorithms, Dig. Signal Process. 42 (2014) 1–26.

[17] T. Oberlin, S. Meignen, S. McLaughlin, Analysis of strongly modulated multicomponent signals with the short-time fourier transform, in: 2013 IEEE International Conference on Acoustics, Speech and Signal Processing (ICASSP), IEEE, pp. 5358–5362.

[18] T. Oberlin, S. Meignen, V. Perrier, The fourier-based synchrosqueezing transform, in: 2014 IEEE International Conference on Acoustics, Speech and Signal Processing (ICASSP), IEEE, pp. 315–319.

[19] M.I. Skolnik, Cinii books - radar handbook, Radar Handbook (1970).

[20] J.W. Pitton, L.E. Atlas, P.J. Loughlin, Applications of positive time-frequency distributions to speech processing, IEEE Trans. Speech Audio Process. 2 (1994) 554–566.

[21] E.J. Candes, P.R. Charlton, H. Helgason, Detecting highly oscillatory signals by chirplet path pursuit, Appl. Comput. Harmonic Anal. 24 (2008) 14–40.

[22] W. Yang, P.J. Tavner, C.J. Crabtree, Y. Feng, Y. Qiu, Wind turbine condition monitoring: technical and commercial challenges, Wind Energy 17 (2014) 673–693.

[23] Z. Feng, M. Liang, Fault diagnosis of wind turbine planetary gearbox under nonstationary conditions via adaptive optimal kernel time–frequency analysis, Renewable Energy 66 (2014) 468–477.

[24] J. Palma, F. Castro, L. Ribeiro, A. Rodrigues, A. Pinto, Linear and nonlinear models in wind resource assessment and wind turbine micro-siting in complex terrain, J. Wind Eng. Ind. Aerodyn. 96 (2008) 2308–2326.

[25] C. Li, M. Liang, A generalized synchrosqueezing transform for enhancing signal time–frequency representation, Signal Process. 92 (2012) 2264–2274.

[26] S. Wang, X. Chen, G. Cai, B. Chen, X. Li, Z. He, Matching demodulation transform and SynchroSqueezing in time-frequency analysis, EEE Trans. Signal Process. 62 (2014) 69–84.

[27] X. Chen, Z. Feng, Iterative generalized time-frequency reassignment for planetary gearbox fault diagnosis under nonstationary conditions, Mech. Syst. Signal Process. 80 (2016) 429–444.

[28] P. Chen, K. Wang, M.J. Zuo, A generalized synchroextracting transform for fast and strong frequency modulated signal analysis, Condit. Monitor. Diagnost. Eng. Manage. (2018) 189–196.

[29] T. Oberlin, S. Meignen, V. Perrier, The fourier-based synchrosqueezing transform, IEEE (2014) 315–319.

[30] T. Oberlin, S. Meignen, V. Perrier, Second-order synchrosqueezing transform or invertible reassignment? towards ideal time-frequency representations, IEEE Trans. Signal Process. 63 (2015) 1335–1344.

[31] F. Auger, P. Flandrin, Improving the readability of time-frequency and time-scale representations by the reassignment method, IEEE Trans. Signal Process. 43 (1995) 1068–1089.

[32] F. Auger, E. Chassande-Mottin, P. Flandrin, Making reassignment adjustable: The Levenberg-Marquardt approach, in: 2012 IEEE International Conference on Acoustics, Speech and Signal Processing (ICASSP), pp. 3889–3892.

[33] R.G. Baraniuk, P. Flandrin, A.J.E.M. Janssen, O.J.J. Michel, Measuring time-frequency information content using the renyi entropies, IEEE Trans. Inf. Theory 47 (2001) 1391–1409.

[34] S. Aviyente, W.J. Williams, Minimum entropy time-frequency distributions, IEEE Signal Process. Lett. 12 (2005) 37–40.

[35] R.A. Carmona, W.L. Hwang, B. Torrésani, Multiridge detection and time-frequency reconstruction, IEEE Trans. Signal Process. 47 (2015) 480–492.